Journal of Electronic Research and Application, 2026, Volume 10, Issue 2
http://ojs.bbwpublisher.com/index.php/JERA
ISSN Online: 2208-3510
ISSN Print: 2208-3502

Design of a Seafloor Geohazard Dynamic Monitoring Device Based on Inertial Navigation System

Haiqing Gu[1], Ran Li[1], Zhipeng Chi[1], Lang Qin[1], Yunsong Hua[1], Hui Yang[1,2], Erliang Xiao[1]

[1]School of Optical-Electrical and Computer Engineering, University of Shanghai for Science and Technology, Shanghai 200093, China
[2]College of Medical Instrumentation, Shanghai University of Medicine & Health Sciences, Shanghai 201318, China

Abstract: To address the deficiency of existing technologies in long-term, large-scale in-situ seafloor geohazard monitoring, a dynamic monitoring device based on an inertial navigation system was designed. It features a three-level architecture with MPU9250 nine-axis sensors, RS485 multi-node communication and independent power supply. An algorithm system combining Euler angle-rotation matrix transformation, Mahony attitude solution and multi-filtering methods was built to realize sensor data denoising, attitude calculation and trajectory reconstruction. Laboratory static and dynamic free-release impact experiments under different inclined angles were conducted for verification. The results show that the device achieves drift-free static data acquisition, accurate and stable dynamic data collection and transmission, and can precisely reconstruct the 3D motion trajectory of monitoring terminals, with the impact acceleration within the measuring range. It meets the basic requirements for seafloor geohazard monitoring and provides a new technical solution for relevant in-situ monitoring.

Keywords: Inertial navigation system; Seafloor geohazard monitoring; MPU9250; Attitude solution; Rotation matrix; Dynamic experiment

Online publication: March 31, 2026

1. Introduction

Marine geological hazards are a type of disaster caused by submarine geological processes. The expansion of engineering constructions such as coastal ports, waterways, submarine pipelines, and optical cables has led to a further increase in the risk of marine geological hazards. Moreover, they are highly prone to inducing a series of secondary disasters, forming disaster chains that exacerbate disaster events [1].

Gas hydrates (combustible ice) are solid substances formed by natural gas (mainly methane) and water under low-temperature and high-pressure environments, usually existing in submarine sediments or permafrost layers [2]. The presence of gas hydrates can enhance the stability of submarine sediments. Changes in environmental conditions may cause the decomposition of gas hydrates [3]. During the mining process, if the temperature and pressure in the

mining area are not effectively controlled, hydrates may transform from a solid state into gaseous state and water. The disappearance of the solid structure of hydrates may cause the originally stable submarine sediments to lose support, thereby triggering geological hazards such as submarine landslides and mudslides [4]. Landslides may affect infrastructure such as submarine cables and pipelines, and even cause damage to marine ecosystems [5]. In engineering projects, accurate monitoring of submarine geological hazards can help engineers reasonably plan engineering routes, avoid the impact of factors such as topographic relief and submarine geological conditions on engineering construction and operation, and also help identify potential risks of submarine geological hazards, such as submarine landslides, tsunamis, and earthquakes, providing an important basis for marine environmental protection and coastal zone management. Therefore, it is necessary to monitor submarine geological hazards.

So far, most characteristics of marine geological hazards can be detected and identified, but it is difficult to effectively monitor them for a long time relying on existing technologies. In-situ monitoring of marine geological hazards requires more stringent technical capabilities, especially the in-situ monitoring of sudden marine geological hazards is more difficult [1]. Currently, the monitoring technologies for submarine geological hazards mainly include MEMS sensor arrays, Ocean Bottom Seismometers (OBS), optical fiber sensing technology, multi-beam bathymetry systems, sonar imaging technology, submarine observation networks, autonomous underwater vehicles (AUV), buoy monitoring systems, and satellite remote sensing technology.

Among them, MEMS sensors are mainly composed of accelerometers, gyroscopes, and magnetometers, and have a wide range of applications, including precision-guided weapons, unmanned aerial vehicles, and the medical field. With the development of accelerometers and gyroscopes, inertial navigation systems have gradually become a research hotspot due to their advantages of small size, light weight, low power consumption, low cost, and impact resistance [6]. In the field of submarine geological hazard monitoring, MEMS sensor arrays are used to monitor marine terrain subsidence and deformation, enabling long-term monitoring. However, the current MEMS sensor arrays are mainly linear arrays, making it difficult to achieve large-scale geological hazard monitoring.

In-situ monitoring technology for marine geological hazards has become a key support for ensuring the safety of coastal cities and the development of the marine economy, as it can directly reveal the triggering mechanisms and evolution processes of hazards [7,8]. Early studies focused on the basic detection of single disaster types, and later gradually expanded to multi-element collaborative monitoring, long-term stable observation, and disaster chain early warning. The ocean bottom seismometer (OBS) developed by Germany's GeoPro company has a maximum operating water depth of 6700 m and can continuously monitor for 6 months, providing core equipment support for global marine earthquake and tsunami early warning [9–11]. The Piezometer series of pore pressure monitoring probes from the French Research Institute for Exploitation of the Sea (IFREMER) are widely used in research on submarine landslides, gas hydrate decomposition, etc., and their upgraded penetration device can achieve in-situ monitoring at a depth of 50m under the seabed [12,13]. In addition, distributed acoustic sensing (DAS) technology realizes high spatial resolution seismic monitoring through submarine communication optical cables, and the monitoring effect is comparable to that of coastal seismic stations [14]. The long-term submarine borehole monitoring equipment (LTBMS) developed in Japan has a monitoring depth of 100m, and integrates multiple types of sensors to independently or jointly monitor crustal movements and sediment deformation [15].

Domestic scholars have achieved remarkable results in the independent research and development of monitoring technologies and their engineering applications. The cable-based submarine seismic observation station (network) developed by the Institute of Geology and Geophysics, Chinese Academy of Sciences, has realized long-term continuous observation of internal Earth processes, providing an innovative platform

for marine earthquake early warning [16]. The SEEGeo system developed by Ocean University of China can realize 12-month continuous monitoring of parameters such as pore pressure and temperature at a depth of 3m in 1500m water depth [17–19]. Other studies, such as the optical fiber submarine seismometer from the Institute of Semiconductors, Chinese Academy of Sciences, and the in-situ real-time automatic observation equipment for submarine deformation and sliding from Ocean University of China, have all shown high reliability in complex marine environments [19–21]. At the same time, the high-density resistivity probe and the comprehensive observation system of the submarine boundary layer from Ocean University of China have realized the synchronous measurement of suspended matter concentration and dynamic changes of the seabed interface, providing a new means for erosion and siltation monitoring [17,18,22].

Therefore, this paper designs a geological hazard monitoring device based on an inertial navigation system to realize long-term and large-scale geological hazard monitoring. In order to verify the function of the device and its feasibility for submarine geological hazard monitoring, an experimental platform is built in the laboratory. The single connecting rod structure of the device is mainly used to design experiments, simulate the static measurement and dynamic release processes of the device, and verify the performance of the inertial navigation system sensors.

2. System design

2.1. System architecture

The structure of the submarine geological disaster monitoring device consists of a central control unit, secondary nodes, and motion monitoring terminals. The central control unit is connected to the secondary nodes via a primary connecting rod, which has a length of 3 meters. The secondary node is connected to three motion monitoring terminals through three secondary rods, each with a length of 1 meter. When all connecting rods are fully extended in the horizontal position, the angles between each pair of the three secondary rods connected to the secondary node are 90° each.

It is planned to use a 12V switching power supply, and the power supplies of each node and terminal are independent of each other to avoid affecting the detection process due to power supply issues. The central control unit, motion monitoring terminals, and secondary nodes are all equipped with nine-axis motion sensors to measure three-axis angular velocity and three-axis acceleration. A scaled-down simulation device was designed based on the structural design of the mechanical device, and the structural schematic diagram is shown in **Figure 1**. In order to verify the data stability and functional feasibility of the system under different conditions, it is necessary to conduct laboratory simulation verification experiments on the system.

Figure 1. Schematic diagram of the connecting rod structure of the simulation device.

2.2. Device connection

The submarine geological disaster monitoring device includes a power module, a data acquisition module, a system control module, and a communication module. Since submarine terrain reconstruction and geological disaster monitoring require data from multiple points within a range, the data acquisition module is designed as a central control unit, a secondary node, and three motion monitoring terminals, with each node capable of independently collecting data. The data acquisition module is connected to the system control module. The system control module is connected to the upper computer via the communication module, and the power module supplies power to the entire system. Each group of experiments can collect data from 5 points. By conducting multiple groups of data collection and processing in a certain arrangement within the range, the coordinates of multiple data points can be obtained.

The secondary node and the motion monitoring terminal have the same structure, but their connection and communication methods are different. The circuit board includes a control chip and an MPU9250 nine-axis motion sensor. The MPU9250 is a nine-axis motion tracking device that integrates a 3-axis gyroscope, a 3-axis accelerometer, and a 3-axis magnetometer. The attitude information, namely the three-axis acceleration and Euler angles, is obtained by resolving the data from the gyroscope and accelerometer. The three-axis coordinate values at that location are calculated through the tilt angle of the rod and the positional relationship, which are then used for submarine terrain reconstruction and geological disaster monitoring. The system control module serves as the central control unit. The control chips of each node read data from the attitude sensor via the IIC protocol, and data transmission between each node adopts the RS485 serial protocol. The communication module is a USB-to-RS485 communication module converter. The power module uses an independent 12V switching power supply to supply power to the other modules.

Each motion monitoring terminal is connected to an RS485 bus and respectively connected to the secondary node. The secondary node is connected to two RS485 buses, one of which (RS485A) is connected to the three motion monitoring terminals, and the other (RS485B) is connected to the central control unit. The central control unit contains two RS485 buses: one is connected to the secondary node and acts as the host to send data reading instructions to and receive data from the motion monitoring terminals; the other is connected to the upper computer via the USB-to-RS485 communication module converter to send data and receive instructions from the upper computer. The power lines of each motion monitoring terminal are connected to the power line of the secondary node, and they are respectively connected to the switching power supply together with the power line of the central control unit.

2.3. Data collection process

After receiving the data reading instruction, the accelerometers and gyroscopes of the attitude sensors on the three motion monitoring terminals respectively collect the original data of three-axis acceleration and three-axis angular velocity. The control chip reads the data through IIC communication, and then sends the data to the secondary node through the RS485 bus. The attitude sensor on the secondary node also collects data. The control chip reads the data through IIC communication, and then sends this data together with the data sent by the three motion monitoring terminals to the central control unit through the RS485 bus. The central control unit receives a total of 4 data. The attitude sensor in the central control unit can also collect data, making a total of 5 data. The control chip of the central control unit has a built-in attitude calculation and filtering program, which can calculate the data sent by the secondary node. Finally, the original data of angular velocity and acceleration or the calculated

three-axis Euler angles and three-axis acceleration data are sent to the upper computer through the communication line and displayed. The data collection process of each node is synchronous and sent to the upper computer in real time. The data collected by MPU9250 can be transmitted to the upper computer in real time through RS485 communication, or stored in the memory of each node and sent to the upper computer through the serial port. The data collection frequency can be adjusted, with the maximum being 1kHz.

3. Algorithm flow

3.1. Euler angles and rotation matrices

Euler angles are a set of three independent angular parameters used to uniquely determine the position of a rigid body undergoing fixed-point rotation. They describe the attitude of an object in three-dimensional space through rotation angles around three coordinate axes. The corresponding three angles are: Yaw angle: the angle of rotation around the Z-axis, Pitch angle: the angle of rotation around the Y-axis, and Roll angle: the angle of rotation around the X-axis.

According to **Equation (1)**, the rotation matrix is a 3x3 matrix R, which is used to describe the rotation of an object in three-dimensional space. According to **Equation (2)**, vectors can be transformed from one coordinate system to another through matrix multiplication. Each column of the rotation matrix represents the direction of the coordinate axis after rotation. Euler angles and rotation matrices can be converted into each other.

$$R = \begin{bmatrix} r_{11} & r_{12} & r_{13} \\ r_{21} & r_{22} & r_{23} \\ r_{31} & r_{32} & r_{33} \end{bmatrix} \tag{1}$$

$$\begin{bmatrix} x_2 \\ y_2 \\ z_2 \end{bmatrix} = R \begin{bmatrix} x_1 \\ y_1 \\ z_1 \end{bmatrix} \tag{2}$$

A rotating coordinate system refers to a coordinate system that rotates around a certain axis in space. By rotating the coordinate system, the description of an object in different reference frames will change. When rotating a coordinate system, the order of rotation is very important. According to different orders of coordinate axis rotation, there are 6 sets of rotation orders in a three-dimensional coordinate system.

According to **Equation (3)**, internal rotation means that the rotation is performed relative to the object's own coordinate system (local coordinate system), and the rotation axis changes with the reference frame rotating with the object.

$$(R_{inner} = R_z(\phi) \cdot R_y(\theta) \cdot R_x(\psi)) \tag{3}$$

Conversion from Euler angles to rotation matrix: For Euler angles in the Z, Y, X order (Yaw: ϕ, Pitch: θ, Roll: ψ), the rotation matrix R can be constructed through the following steps. According to **Equation (4)**, **(5)**, and **(6)**, the rotation matrices for rotation around the Z-axis (Yaw), rotation around the Y-axis (Pitch), and rotation around the X-axis (Roll) are respectively:

$$R_z(\phi) = \begin{bmatrix} cos\phi & -sin\phi & 0 \\ sin\phi & cos\phi & 0 \\ 0 & 0 & 1 \end{bmatrix} \tag{4}$$

$$R_y(\theta) = \begin{bmatrix} cos\theta & 0 & sin\theta \\ 0 & 1 & 0 \\ -sin\theta & 0 & cos\theta \end{bmatrix} \tag{5}$$

$$R_x(\psi) = \begin{bmatrix} 1 & 0 & 0 \\ 0 & cos\psi & -sin\psi \\ 0 & sin\psi & cos\psi \end{bmatrix} \quad (6)$$

According to **Equation (3)** and **(7)**, the final rotation matrix R is the product of three rotation matrices. The nine elements in **Equation (1)** and **(7)** correspond one-to-one. The rotation matrix can be calculated from Euler angles, and it can be used for coordinate transformation or attitude description. Through the rotation matrix and the positional relationship of the rod, the attitude and motion trajectory of the attitude sensor can be obtained.

$$R = R_z(\phi)R_y(\theta)R_x(\psi) = \quad (7)$$

$$\begin{bmatrix} \cos\theta\cos\phi & \sin\psi\sin\theta\cos\phi - \cos\psi\sin\theta & \cos\psi\sin\theta\cos\phi + \sin\psi\sin\phi \\ \cos\theta\sin\phi & \sin\psi\sin\theta\sin\phi + \cos\psi\cos\phi & \cos\psi\sin\theta\sin\phi - \sin\psi\cos\theta \\ -\sin\theta & \sin\psi\cos\theta & \cos\psi\cos\theta \end{bmatrix}$$

3.2. Attitude calculation and filtering algorithm

In an attitude sensor, the raw data from the accelerometer and gyroscope can be processed through attitude calculation to obtain acceleration and angle data. The Mahony complementary filtering quaternion algorithm corrects the errors of the gyroscope using the accelerometer. Then, it calculates the quaternion based on the corrected three-axis angular velocity, and further computes the Euler angles of the sensor from the quaternion. Finally, a rotation matrix is constructed using the Euler angles for coordinate transformation, converting the three-axis acceleration data in the sensor coordinate system to that in the laboratory coordinate system.

During dynamic experiments, the movement and impact process of the rod will cause large-amplitude vibrations, which are affected by low-frequency noise. Therefore, high-pass filtering is used to remove the DC drift and low-frequency noise of the sensor, while retaining the high-frequency dynamic components. In communication systems, high-pass filtering separates high-frequency carriers from low-frequency interference to improve the signal-to-noise ratio. For a high-pass filter, is the cutoff frequency; f > fc is the passband, and f < fc is the stopband. The Nyquist frequency is a characteristic parameter of the sampling system, referring to half of the sampling frequency fs, i.e., fN = fs/2. It is the upper limit of the highest signal frequency that ensures the sampled signal can be restored without distortion.

4. Free release dynamic experiment

The nine-axis motion sensor can output information such as the angular velocity and acceleration of the carrier. The schematic diagram of the positive directions of the three axes of MPU9250 is shown in **Figure 2**. Each sensor is installed in the device with their three-axis positive directions aligned. Due to the limitation of the mechanical structure, the connecting rod can only move in a two-dimensional plane. Therefore, among the three-axis attitude angles obtained through attitude calculation from the three-axis angular velocity measured by the sensor, the pitch angle is equal in magnitude to the inclination angle of the connecting rod, so the inclination angle of the connecting rod can be obtained. By collecting static data from the sensor for a long time and analyzing the errors, it is found that because Kalman filtering is added before attitude calculation, the data collected by the sensor over a long time range has no obvious drift, which verifies the feasibility of the sensor in long-term terrain monitoring applications.

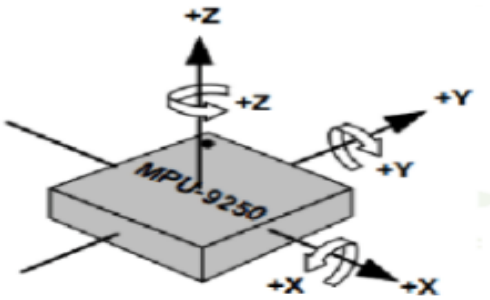

Figure 2. Diagram of MPU9250 three-axis positive directions.

After being dropped from the sea surface, the seabed geological disaster monitoring device first undergoes a dynamic release and impact process, and then statically collects topographic data. During the dynamic process, collisions occur when the probe penetrates the seabed surface, and also when the connecting rods respectively land on the seabed surface. During the collision process, the angular velocity and acceleration collected by the sensors will change over a large range in a short time. Due to the complexity of the seabed topography, the inclination angles of different connecting rods after landing on the seabed surface are also different. Therefore, it is necessary to analyze the dynamic process of the device, and conduct experimental simulation, data collection and processing on the release and impact processes of the secondary rods.

The experiment needs to test whether the sensor data is accurate during the dynamic change process, and whether there will be a large drift after a period of time after the collision. Then, in the laboratory, simulate the process where one end of a single secondary rod is fixed, and the other end is released at a certain initial angle and falls onto a horizontal plane and inclined planes at different angles. The original data of the three-axis angular velocity and acceleration during the release and collision processes was collected. Through attitude calculation, the data of the sensor's three-axis Euler angles and acceleration changing with time during the entire process can be obtained. Through the rotation matrix, the movement trajectory of the sensor, which is an arc, can be obtained, and the peak value of the acceleration is the acceleration at the moment of impact. The acceleration changes greatly during the impact process, and various situations are verified to ensure that the change range of the acceleration does not exceed the measuring range.

The MPU9250 system board was aligned sequentially along the positive directions of the three axes and installed in the simulation device. The data acquisition frequency was set to 1 kHz, and all auxiliary components were properly connected. The device was powered on in a horizontal direction and securely fixed. One end of the secondary rod, with the MPU9250 system board mounted at its tip, was pulled to a 60° position using a thin string, such that the x- and z-axes remained fixed while rotation occurred about the y-axis.Horizontal and inclined planes at angles of 20°, 0°, −40°, and −60° were prepared, and their inclination angles were verified using an electronic protractor. The thin string was then released, allowing the secondary rod with the MPU9250 system board at its end to fall freely, impact the horizontal or inclined plane, and eventually come to rest. Data were continuously collected and transmitted from the moment of power-on through the entire process, including the release of the secondary rod, its free fall, the impact of its end with the horizontal or inclined plane, and its eventual stabilization. The experimental procedure was recorded using a high-speed camera, as illustrated in **Figure 3**. The feasibility of the device under dynamic conditions was thereby evaluated, along with the accuracy of attitude sensor data acquisition during the release and impact phases, and the stability of data transmission. Subsequent error analysis

and data processing were also performed.

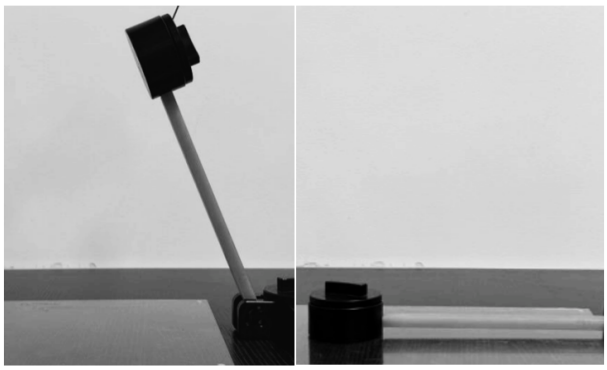

Figure 3. High-speed camera image of dynamic experiment of free release of simulation device. Experimental diagram before free release (left). Experimental diagram after free release (right).

For four sets of dynamic experiments involving inclined planes at different angles and a horizontal plane, the gyroscope and accelerometer in the MPU9250 collected three-axis angular velocity data and three-axis raw acceleration data respectively. To make the data smoother, Kalman filtering was applied to the three-axis angular velocity and three-axis raw acceleration data, resulting in filtered raw data. Then, the quaternion method was used for attitude calculation to obtain three-axis Euler angles and three-axis acceleration data.

Figure 4 shows the pitch angle data graphs of the four sets of experiments. In each set of experiments, the curves of the rod from release to just before impact almost overlap. For the rod released from a 60° angle, the pitch angle during its falling phase can be fitted using the same function.

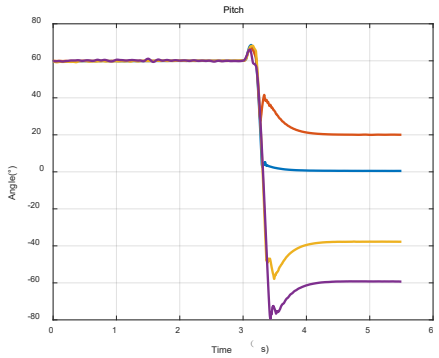

Figure 4. Pitch angle data plots for the four experimental groups.

The following experimental results all take the -60°inclined plane as an example. The data graphs of the three-axis angular velocity and Euler angles are shown in **Figure 5**.

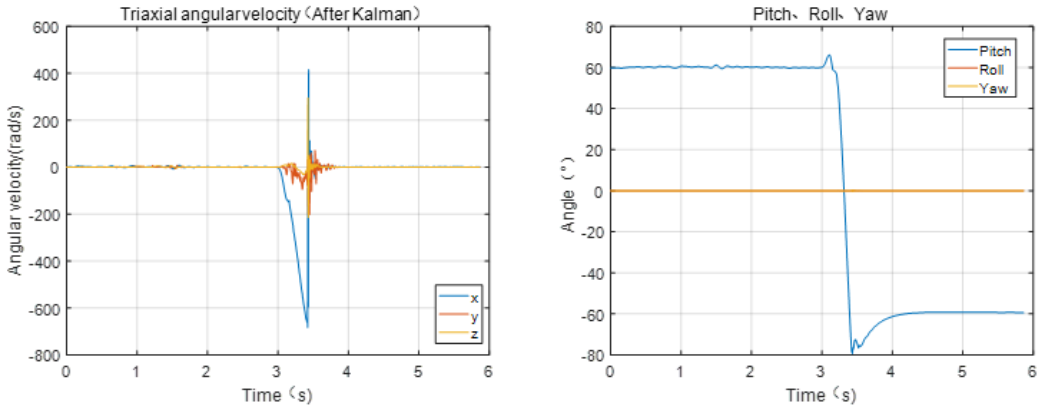

Figure 5. Experimental data graph. Three-axis angular velocity data graph (left). Euler angle data graph (right).

According to **Equation (4)**, **(5)**, and **(6)**, the rotation matrices around the z-axis (Yaw), y-axis (Pitch), and x-axis (Roll) at each moment are calculated using the three-axis Euler angles. The rotation order is first around the z-axis, then around the y-axis, and finally around the x-axis. According to **Equation (3)** and **(7)**, the total rotation matrix is calculated. The initial position vector of the motion monitoring terminal at the end of the secondary rod is set as (1, 0, 0). According to **Equation (2)**, the rotation matrix is multiplied by the initial position vector of the rod on the left, and the resulting value is the coordinate of the motion monitoring terminal at each moment. All coordinates are plotted and connected, as shown in **Figure 6**, to obtain the three-dimensional motion trajectory of the motion monitoring terminal during the entire dynamic process.

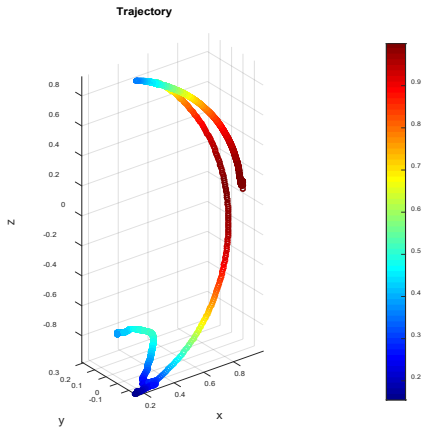

Figure 6. 3D trajectory diagram.

4. Conclusion

This paper designed an inertial navigation-based seafloor geohazard monitoring device and completed its laboratory verification. The three-level hardware architecture realizes multi-node and high-frequency data acquisition, solving the problem of limited monitoring range of traditional sensors. The proposed algorithm system supports accurate data processing, attitude analysis and trajectory reconstruction for seafloor geohazard dynamic monitoring. Static and dynamic experiments verify the device's good stability, accuracy and dynamic adaptability,

which meets the basic technical requirements for long-term and large-scale seafloor geohazard monitoring, providing a new in-situ monitoring solution. This research is still in the laboratory stage, without considering the extreme deep-sea environment and the cumulative error of single inertial sensors. In the follow-up, the device's structural and protective design will be optimized for deep-sea adaptability tests. Multi-source data fusion with other sensing technologies will be explored to reduce measurement errors and improve monitoring accuracy. The networking and remote transmission capabilities will be enhanced to promote the engineering application of the device, providing technical support for marine engineering safety and seafloor geohazard early warning.

Disclosure statement

The author declares no conflict of interest.

References

[1] Jia Y, Chen T, Li P, et al., 2022, Research Progress on In-Situ Monitoring Technologies for Marine Geohazards. The Chinese Journal of Geological Hazard and Control, 33(3): 1–14.

[2] Shen P, 2021, Experimental Study on Seepage of Natural Gas Hydrate-Bearing Sediments and Stimulation Methods, thesis, Chongqing University.

[3] Ma W, 2011, Analysis of Risk Factors in the Development of Natural Gas Hydrates in the South China Sea, thesis, Ocean University of China.

[4] Yu F, 2011, Study on Mechanical Properties of Methane Hydrate and its Sediments, thesis, Dalian University of Technology.

[5] Li Y, 2023, Study on Mechanical Mechanism and Disaster-Causing Mechanism of Debris Flow-Turbidity Current Transformation Process of Submarine Landslide, thesis, China University of Geosciences.

[6] Han L, 2019, Research on Algorithms of Micro Integrated Navigation System based on MEMS IMU, thesis, Nanjing University of Science and Technology.

[7] Kopp H, Chiocci F, Bernd T, et al., 2021, Marine Geohazards: Safeguarding Society and the Blue Economy from a Hidden Threat, European Marine Board Publishing, Belgium.

[8] Favali P, Beranzoli L, 2009, Seafloor Observatory Science: A Review. Annals of Geophysics, 49(2/3): 515–567.

[9] Gohl K, 2003, Structure and Dynamics of a Submarine Continent: Tectonic-Magmatic Evolution of the Campbell Plateau (New Zealand), Alfred-Wegener-Institut für Polar-und Meeresforschung, Germany.

[10] Wallace L, Araki E, Saffer D, et al., 2016, Near-Field Observations of an Offshore Mw 6.0 Earthquake from an Integrated Seafloor and Subseafloor Monitoring Network. Journal of Geophysical Research: Solid Earth, 121(11): 8338–8351.

[11] Papoulia J, Makris J, Koulakov I, et al., 2018, Microseismicity and Crustal Deformation of the Dodecanese Volcanic Area. Bollettino di Geofisica Teorica ed Applicata, 55(2): 281–302.

[12] Sultan N, Savoye B, Jouet G, et al., 2010, Investigation of a Possible Submarine Landslide at the Var Delta Front. Canadian Geotechnical Journal, 47(4): 486–496.

[13] Stegmann S, Sultan N, Garziglia S, et al., 2012, A Long-Term Monitoring Array for Landslide Precursors, OTC, 1–10.

[14] Sladen A, Rivet D, Ampuero J, et al., 2019, Distributed Sensing of Earthquakes on Seafloor Telecom Cables. Nature Communications, 2019(10): 5777.

[15] Araki E, Saffer D, Kopf A, et al., 2017, Recurring and Triggered Slow-Slip Events near the Trench at the Nankai

Trough. Science, 356(6343): 1157–1160.

[16] Hao T, You Q, 2011, Development Status of Domestic Ocean Bottom Seismometers and their Application in Seafloor Structure Detection. Chinese Journal of Geophysics, 54(12): 3352–3361.

[17] Liu T, Wei G, Kou H, et al., 2019, Pore Pressure Observation: Pressure Response of Probe Penetration and Tides. Acta Oceanologica Sinica, 38(7): 107–113.

[18] Guo L, 2016, Research on the Development and Application of an In-Situ Comprehensive Observation System for the Seafloor Boundary Layer, thesis, Ocean University of China.

[19] Zhang W, Huang W, 2018, Development and Application Exploration of Optical Fiber Ocean Bottom Seismometer, National Security Geophysics Professional Committee of Chinese Geophysical Society, Xi'an Cartographic Publishing House, 296–300.

[20] Wang Z, Sun Y, Jia Y, et al., 2020 Wave-Induced Seafloor Instabilities in the Subaqueous Yellow River Delta. Landslides, 17(8): 1849–1862.

[21] Jia Y, Wang Z, Liu X, et al., 2017, The Research Progress of Field Investigation and In-Situ Observation Methods for Submarine Landslide. Periodical of Ocean University of China, 47(10): 61–72.

[22] Traykovski P, Hay A, Irish J, et al., 1999, Geometry, Migration, and Evolution of Wave Orbital Ripples at LEO15. Journal of Geophysical Research: Oceans, 104 (C1): 1505–1524.